

196

NACA TN 2585

NATIONAL ADVISORY COMMITTEE FOR AERONAUTICS

TECHNICAL NOTE 2585

CALCULATION OF AERODYNAMIC FORCES ON A
PROPELLER IN PITCH OR YAW

By John L. Crigler and Jean Gilman, Jr.

Langley Aeronautical Laboratory
Langley Field, Va.



Washington

January 1952

AFM-C
TECHNICAL LIBRARY
AFL 2811





0065522

NATIONAL ADVISORY COMMITTEE FOR AERONAUTICS

TECHNICAL NOTE

CALCULATION OF AERODYNAMIC FORCES ON A
PROPELLER IN PITCH OR YAW¹

By John L. Crigler and Jean Gilman, Jr.

SUMMARY

An analysis has been made to determine the applicability of existing propeller theory and the theory of oscillating airfoils to the problem of determining the magnitude of the forces on propellers in pitch or yaw. Strip calculations including the Goldstein correction factors and using compressible airfoil characteristics were first made as though steady-state conditions existed successively at several blade positions of the propeller blades during one revolution. A theory of oscillating airfoils in pulsating incompressible linearized potential flow was then considered from which it was possible to determine factors which would modify the forces as calculated under the assumption of steady-state compressible flow.

Comparisons of the steady-state calculations with experimental results show that the magnitude of the force changes experienced by the blades can be predicted with satisfactory accuracy. Results of calculations made by the oscillating theory indicate that the actual forces on the blade may be somewhat lower than the values calculated by the steady-state method. It was not possible to establish this conclusion definitely because of the lack of sufficient experimental data for comparison.

The turning moment on the shaft of a two-blade propeller fluctuates between approximately zero and its maximum value twice per revolution. For the operating condition investigated the turning moment on the shaft of a three-blade propeller remains nearly constant at about 75 percent of the maximum value attained with the two-blade propeller.

INTRODUCTION

Large-diameter propellers incorporating thin blade sections are becoming a necessity for certain aircraft installations using large unit

¹Supersedes the recently declassified NACA RM L8K26, "Calculation of Aerodynamic Forces on a Propeller in Pitch or Yaw" by John L. Crigler and Jean Gilman, Jr., 1949.

power plants at high altitude and high speed. On such propeller installations, the oscillating air forces due to yaw or pitch of the propeller axis may cause dangerous vibratory stresses with a frequency of once per revolution. The airfoil blade section experiences oscillating air forces that vary with the position of the blade around the periphery. These air forces on the propeller blade section in flight must be related to the proper Mach number, advance ratio, blade-section lift coefficient, inclination of the propeller shaft axis to its forward motion, and the wave length of the oscillation. A knowledge of the air forces on the blade section as a function of the propeller operating conditions is needed in a study of the problem. No existing theory completely describes the operating condition of a pitched or yawed propeller.

In this paper the air forces on the propeller blades are calculated first under the assumption that the existing propeller theory may be used in conjunction with the instantaneous angles of attack and resultant velocities along the blades of the pitched propeller at successive blade positions around the periphery. This method, herein termed the "steady-state" method, permits the use of the usual steady-state compressible airfoil characteristics with the Goldstein correction factors for a finite number of blades. Then several aspects of the nature of the forces developed by an oscillating airfoil are considered. Expressions based on linearized theory for calculating the air forces on a two-dimensional thin flat-plate airfoil oscillating in angle of attack in a steady stream in a nonviscous incompressible fluid were developed in reference 1. Some modifications to this theory were presented in reference 2 to permit calculations when the stream velocity as well as the angle of attack varied with time. The expressions of reference 2 are used to estimate the changes of the airfoil characteristics in a compressible oscillating flow field.

Very little experimental data with which to compare the results of these calculations are available. The steady-state compressible characteristics are computed for the propeller tested in reference 3, however, and are compared with the experimental data given therein. The calculations are made for two-blade and three-blade single-rotating propellers and satisfactory agreement with the available experimental data is obtained.

SYMBOLS

- | | |
|---|---|
| a | distance to center of rotation from midchord of airfoil,
feet (fig. 2) |
| B | number of blades |
| c | chord, feet |

c_d	profile drag coefficient
c_l	two-dimensional lift coefficient
$C(k) = F + iG$	C function (reference 1)
C_T	thrust coefficient $\left(\frac{T}{\rho n^2 D^4} \right)$
$\frac{dC_T}{dx}$	element thrust coefficient $\left(\frac{dT/dx}{\rho n^2 D^4} \right)$
$\left(\frac{dC_T}{dx} \right)_{wt}$	instantaneous element thrust coefficient $\left(\frac{dT_{wt}/dx}{\rho n^2 D^4} \right)$
D	propeller diameter, feet
h	vertical deflection (flapping) of airfoil, feet (fig. 2)
J	advance ratio (V/nD)
J_{wt_0}	local advance ratio, steady part $(J \cos \alpha_T)$
J_{wt}	instantaneous local advance ratio $\left(\frac{\pi x \cos \alpha_T}{\frac{\pi x}{J} + \sin \alpha_T \sin \omega t} \right)$
$k_{W_{wt}}, k_{\alpha_P}, k_h$	parameter used in determining the function $F + iG$ $\left(k = \frac{\omega c}{2W_0} \right)$
$k_{W_{wt}} + k_{\alpha_P} = \frac{\omega c}{W_0} = k_l$	
L	lift, pounds
L_c	lift coefficient of oscillating airfoil $\left(\frac{L}{2\pi \alpha_{P_0} \frac{\rho W_0^2}{2} c} \right)$
m	turning moment, foot-pounds

m_c	moment coefficient $\left(\frac{m}{\rho V^2 D^3} \right)$
M	Mach number
n	propeller rotational speed, revolutions per second
r	radius to blade section, feet
R	tip radius
t	time, seconds
T	thrust, pounds
T_{wt}	instantaneous thrust, pounds
V	forward velocity of airplane, feet per second
W_0	geometric resultant velocity, steady part, feet per second (fig. 1)
W_{wt}	instantaneous geometric resultant velocity, feet per second
x	fractional radius to propeller blade section $\left(\frac{r}{R} \right)$
x_o	radius ratio at spinner juncture
α	angle of attack, degrees
α_i	angle of inflow, degrees
α_{P_o}	amplitude in oscillation of angle of attack, radians or degrees (fig. 1)
α_P	instantaneous incremental angle of attack of blade section, radians or degrees
α_T	angle of inclination of propeller thrust axis, degrees (fig. 1)
β	blade-angle setting at 0.75 radius, degrees

$$\gamma = \tan^{-1} \frac{c_d}{c_l}$$

ϵ fractional amplitude of stream pulsation $\left(\frac{W_{\omega t_{\max}}}{W_0} - 1 \right)$

κ Goldstein correction factor for finite number of blades

ρ mass density of air, slugs per cubic foot

σ section solidity $\left(\frac{Bc}{2\pi r} \right)$

ϕ_0 local geometric helix angle, steady part, degrees

$$\left(\tan^{-1} \frac{J}{\pi x} \cos \alpha_T \right)$$

$\phi_{\omega t}$ instantaneous geometric helix angle, degrees

$$\left(\tan^{-1} \frac{\cos \alpha_T}{\frac{\pi x}{J} + \sin \alpha_T \sin \omega t} \right)$$

ϕ aerodynamic helix angle, degrees (equation (4))

ω angular velocity of propeller, radians per second
 $(2\pi n)$

A dot over a quantity denotes the first derivative of the quantity with respect to time; two dots, the second derivative with respect to time.

FORCES ON AN INCLINED PROPELLER

The Velocity Diagram

Figure 1(a) shows a side view of a propeller disk, the thrust axis of which is inclined at an angle α_T to the forward velocity V . This forward velocity V is shown resolved into a component $V \cos \alpha_T$ perpendicular to the plane of rotation and a component $V \sin \alpha_T$ parallel to the plane of rotation. Figure 1(b), a view perpendicular to the plane of rotation along the thrust axis, shows the velocity component $V \sin \alpha_T$

at a section of a propeller blade which is located at a position ωt on the propeller disk. In this paper the time variable ωt , which defines the position of the blade, is considered to be zero when the blade is initially vertical upward with the propeller axis in positive pitch and is measured in the direction of rotation (these axes may be rotated to comply with propeller attitudes other than pitch). With this convention the vector $V \sin \alpha_T$ may be resolved into a component $V \sin \alpha_T \sin \omega t$ in the direction of the tangential velocity ωr and a component $V \sin \alpha_T \cos \omega t$ in a radial direction along the blade. In the treatment that follows, the radial component of the flow ($V \sin \alpha_T \cos \omega t$) is assumed to have a negligible effect on the airfoil characteristics. With this assumption, the effect of the periodic change in the rotational velocity ($\pi m D x + V \sin \alpha_T \sin \omega t$) and the component velocity $V \cos \alpha_T$ on the propeller characteristics remain to be determined.

The vector diagram for a section of an inclined propeller is shown in figure 1(c). In this figure the induced effects are not included. It should be realized, however, that the aerodynamic helix angles will be somewhat different from the geometric helix angles shown. From figure 1(c) the geometric helix angle for any position of the propeller blade is given by

$$\phi_{\omega t} = \tan^{-1} \frac{V \cos \alpha_T}{\pi m D x + V \sin \alpha_T \sin \omega t}$$

or

$$\phi_{\omega t} = \tan^{-1} \frac{\cos \alpha_T}{\frac{\pi x}{J} + \sin \alpha_T \sin \omega t} \quad (1)$$

The resultant velocity is given by

$$w_{\omega t} = \sqrt{V^2 \cos^2 \alpha_T + (\pi m D x + V \sin \alpha_T \sin \omega t)^2} \quad (2)$$

From the relationship in equation (1), the local advance ratio is given by

$$J_{\omega t} = \frac{\pi x \cos \alpha_T}{\frac{\pi x}{J} + \sin \alpha_T \sin \omega t} \quad (3)$$

From equation (3), the local advance ratio is seen to vary depending on the position of the blade.

Method of Analysis

In calculating the forces on an inclined propeller it must be realized that not only do the blade sections operate in a variable flow field but that the flow is a compressible one with the possibility of high section Mach numbers along the propeller blades. The method of reference 2 for dealing with the oscillating effects applies to incompressible flow where the slope of the lift curve is approximately 2π , while in the compressible case, the slope may be considerably higher. Since the wave length in oscillating flow is usually several blade chords (10 or more), it appears logical as a first approximation to consider the oscillating effects to be negligible as compared with the change of slope of the lift curve with change in Mach number. Also, the Goldstein correction factors for a finite number of blades have been found to apply reasonably well when applied to the calculation of forces on nonoptimum propellers (reference 4). Therefore, it appears reasonable to extend their use to the present case.

Steady state. - In steady-state calculations of the forces and moments on the blade of a pitched propeller, a change in time (blade position) is treated simply as a change in the operating V/nD of the propeller in accordance with equation (3). The complete propeller is assumed to operate successively at different blade positions under the instantaneous conditions at each particular position. The thrust per blade at each position is determined from

$$\frac{T_{\omega t}}{B} = \frac{\rho n^2 D^4}{B} \int_{x_0}^{l.0} \left(\frac{dC_T}{dx} \right)_{\omega t} dx \quad (4)$$

where

$$\left(\frac{dC_T}{dx}\right)_{\omega t} = \kappa \pi^3 x^3 \frac{\alpha_i}{57.3} \frac{\cot \phi - \tan \gamma}{\left(\cot \phi + \frac{\alpha_i}{57.3}\right)^2} \left(1 + \frac{J}{\pi x} \sin \alpha_T \sin \omega t\right)^2 \quad (5)$$

Equation (5), except for the factor $\left(1 + \frac{J}{\pi x} \sin \alpha_T \sin \omega t\right)^2$, is from reference 4. The quantities ϕ and α_i are determined by the same method as in reference 4 by using the quantity $J_{\omega t}$ (equation (3)) in place of J . The additional factor $\left(1 + \frac{J}{\pi x} \sin \alpha_T \sin \omega t\right)^2$ in equation (5) is needed to put the element thrust gradient $\frac{dC_T}{dx}$ in terms of $\rho n^2 D^4$ rather than in terms of the apparently varying n in $J_{\omega t}$ (equation (3)).

The turning moment (yawing moment of a pitched propeller on the propeller shaft) is the difference in bending moments from the highly loaded side to the lightly loaded side of the inclined propeller. For the steady-force calculations this bending moment reaches a maximum on the two-blade propeller when the blades are in the horizontal plane. The maximum turning moment from the steady-flow calculations is found by graphically integrating

$$x R \rho n^2 D^4 \left[\left(\frac{dC_T}{dx}\right)_{90} - \left(\frac{dC_T}{dx}\right)_{270} \right] dx \quad (6)$$

from the spinner surface to the propeller tip.

Oscillating flow.— The expression for the total lift of an infinitely thin airfoil of infinite aspect ratio oscillating in an incompressible

pulsating stream (see fig. 2) is given by equation (12) of reference 2 (with suitable changes in notation) as

$$\begin{aligned}
 L = -\pi\rho \frac{c^2}{4} & \left[\ddot{h} + W_{wt} \dot{\alpha}_P + \dot{W}_{wt} (\alpha + \alpha_P) - a \frac{c}{2} \ddot{\alpha}_P \right] - \\
 2\pi\rho W_{wt} \frac{c}{2} & \left\{ W_0 \alpha + \epsilon W_0 \alpha C(k_{W_{wt}}) e^{i\omega t} + \right. \\
 & \left[\frac{c}{2} \left(\frac{1}{2} - a \right) \dot{\alpha}_P + W_0 \alpha_P \right] C(k_{\alpha_P}) + h C(k_h) + \\
 & \left. \epsilon W_0 \alpha_P C(k_{W_{wt}} + k_{\alpha_P}) e^{i\omega t} \right\} \quad (7)
 \end{aligned}$$

where

$$W_{wt} - W_0 = W_0 \epsilon e^{i\omega t}$$

$$h = h_0 e^{i\omega t}$$

$$\alpha_P = \alpha_{P_0} e^{i\omega t}$$

$$C(k) = F + iG \quad (\text{see reference 1})$$

In the preceding expressions, ϵ denotes the fractional amplitude of the perturbation part of the stream pulsations, h_0 the amplitude of the vertical displacement (flapping), and α_{P_0} the amplitude of the incremental angle of attack due to the rotation of the airfoil about the point a . The equations defining the quantities $(W_{wt} - W_0)$, h , and α_P describe these quantities as pure sinusoidal variations; it thus becomes necessary to ascertain the applicability of these definitions to the inclined propeller case.

Figure 1 shows that the maximum increment in the geometric angle of attack occurs at the quantity $\sin \omega t = 1$ ($\omega t = 90^\circ$) and at $\sin \omega t = -1$ ($\omega t = 270^\circ$). The amplitude α_{p_0} of the geometric angle of attack at $\omega t = 90^\circ$ is

$$\phi_0 - \phi_{90} = \tan^{-1} \frac{J}{\pi x} \cos \alpha_T - \tan^{-1} \frac{\cos \alpha_T}{\frac{\pi x}{J} + \sin \alpha_T}$$

and the amplitude at $\omega t = 270^\circ$ is

$$\phi_{270} - \phi_0 = \tan^{-1} \frac{\cos \alpha_T}{\frac{\pi x}{J} - \sin \alpha_T} - \tan^{-1} \frac{J}{\pi x} \cos \alpha_T$$

These values have been calculated for several values of $\frac{J}{\pi x}$ with the angle α_T as parameter, and the results are shown plotted in figure 3. In figure 4 are shown results of similar calculations made to determine the value of ϵ at $\omega t = 90^\circ$ and $\omega t = 270^\circ$. Figures 3 and 4 show that in the propeller case the deviation from sinusoidal variations in the resultant velocity and angle of attack is small at thrust-axis angles less than about 6° and values of $\frac{J}{\pi x}$ less than approximately 2.

The flapping motion h is a function of the blade stiffness and will not be considered here. Calculations show that the effect of this motion on the maximum force is in general small but that the lag in the position of the maximum force may become large depending on the frequency of the oscillations.

When the h terms are dropped, equation (7) reduces to

$$L = -\pi \rho \frac{c^2}{4} \left[W_{wt} \dot{\alpha}_P + \dot{W}_{wt} (\alpha + \alpha_P) \right] - 2\pi \rho W_{wt} \frac{c}{2} \left[W_0 \alpha + (W_{wt} - W_0) \alpha C(k_{W_{wt}}) + \left(\frac{c}{4} \dot{\alpha}_P + W_0 \alpha_P \right) C(k_{\alpha_P}) + (W_{wt} - W_0) \alpha_P C(k_{W_{wt}} + k_{\alpha_P}) \right] \quad (8)$$

For the type of motion being considered it will be convenient to assign the following values to the parameters appearing in equation (8):

$$\alpha_p = -ia_{p_0} e^{i\omega t}$$

$$h = 0$$

$$W_{wt} = W_0 (1 - i\epsilon e^{i\omega t})$$

$$\epsilon = \frac{W_{90}}{W_0} - 1$$

$$C(k) = F + iG$$

In the preceding expressions the parameter a_{p_0} is taken as the amplitude of the aerodynamic angle of attack as estimated by steady-state calculations in potential flow. The function $C(k)$ is a complex function of the parameter k (reference 1) and is given by

$$C(k) = F(k) + iG(k)$$

where F and G are obtained from standard Bessel functions of the first and second kinds with argument k . The variation of the functions F and G with the parameter $1/k$ is given in figure 4 and table II of reference 1. In the present case the functions F and G are evaluated as in reference 2 for k 's defined as follows:

$$k_{W_{wt}} = \frac{c\omega_{W_{wt}}}{2W_0}$$

$$k_{\alpha_p} = \frac{c\omega_{\alpha_p}}{2W_0}$$

$$k_{W_{wt}} + k_{\alpha_p} = \frac{(\omega_{W_{wt}} + \omega_{\alpha_p})c}{2W_0}$$

For the case being considered it is assumed that $\omega_{W_{wt}} = \omega_{\alpha_p} = \omega$; therefore, $k_{W_{wt}} = k_{\alpha_p} = k$ and $k_{W_{wt}} + k_{\alpha_p} = k_1 = 2k$. Accordingly, the functions $C(k_{W_{wt}})$ and $C(k_{\alpha_p})$ are equal and are denoted by $C(k) = F + iG$ while the function $C(k_{W_{wt}} + k_{\alpha_p})$ is denoted by $F_1 + iG_1$.

It should be noted that some of the real terms in equation (8) are not multiplied by the $C(k)$ functions. These real terms can be interpreted as giving the total force on the airfoil and the imaginary terms, the force due to perturbation velocities only.

When the real part of equation (8) is taken, the resulting total force coefficient is given by

$$\begin{aligned} L_C &= \frac{L}{\frac{\rho W_0^2}{2\pi c} \frac{c}{\alpha_{p_0}}} = \frac{\alpha}{\alpha_{p_0}} + \left[F \left(1 + \epsilon \frac{\alpha}{\alpha_{p_0}} \right) - \frac{k}{2} G + \epsilon \frac{\alpha}{\alpha_{p_0}} \right] \sin \omega t + \\ &\quad \epsilon \left[k \left(1 + \frac{F}{2} \right) + G \left(1 + \epsilon \frac{\alpha}{\alpha_{p_0}} \right) + G_1 \right] \sin 2\omega t - \epsilon^2 F_1 \sin 3\omega t + \\ &\quad \left[\frac{k}{2} \left(1 + F + \epsilon \frac{\alpha}{\alpha_{p_0}} \right) + G \left(1 + \epsilon \frac{\alpha}{\alpha_{p_0}} \right) \right] \cos \omega t - \\ &\quad \epsilon \left[F \left(1 + \epsilon \frac{\alpha}{\alpha_{p_0}} \right) - \frac{k}{2} G + F_1 \right] \cos 2\omega t - \epsilon^2 G_1 \cos 3\omega t \end{aligned} \quad (9)$$

The lift-force coefficient L_c for propeller-blade computations applies to only one blade element. If the curves from all blades are plotted and integrated and the ordinates summed, the curves thus obtained may be used to determine the turning moment on the propeller shaft as a function of time. The turning moment on the shaft (yawing moment for pitched propeller) for any position is found by plotting the lift force at each blade element times its moment arm and integrating graphically.

CALCULATION OF FORCES AND DISCUSSION OF RESULTS

Steady state. - The calculations were made for a 4-foot-diameter propeller having an NACA 4-(3.9)(07)-0345-B blade design of NACA 16-series sections. A description of the propeller and blade-form curves is given in reference 3. The calculations made, assuming steady flow, were for a two-blade propeller for blade angles of 26° and 53° measured at the 0.75 radius, for a free-stream Mach number of 0.30, and for the propeller thrust axis inclined at an angle of 4° . For each operating condition of the propeller there is a variation of Mach number along the blade which must be taken into account. The airfoil data used were taken from reference 5 but, since the highest Mach number covered in the report was 0.7, extrapolation of the airfoil data to Mach numbers as high as 0.9 was necessary. The lift characteristics for a Mach number of 0.6 were used to extrapolate to higher Mach numbers. The extrapolation was made by holding the angle of zero lift obtained at $M = 0.6$ constant and changing the slope of the lift curve by the Prandtl-Glauert relationship

$$\left(\frac{dc_l}{d\alpha} \right)_M = \left(\frac{dc_l}{d\alpha} \right)_{M=0.6} \frac{\sqrt{1 - (0.6)^2}}{\sqrt{1 - M^2}}$$

Figure 5 gives a comparison of the variation of the calculated and the wake-survey thrust coefficients with respect to the blade position ωt at $J = 1.2$ for a blade-angle setting of 26° and a thrust-axis angle α_T of 4° . Figure 6 gives a similar comparison at $J = 2.8$, $\beta = 53^\circ$, and $\alpha_T = 4^\circ$, and figure 7 at $J = 3.1$ for $\beta = 53^\circ$ and $\alpha_T = 4^\circ$. The maximum and minimum calculated instantaneous thrust coefficients differ slightly from the measured values in all cases. There

is also a rather large phase difference in the position of the maximum calculated and measured thrust coefficient at the value $J = 1.2$. The position of the survey rake for the experimental data of reference 3 was changed to get each individual point rather than making simultaneous measurements of a number of points for each particular operating condition.

At the same time that the experimental rake survey data were taken force-test thrust coefficients were measured. A study of these data revealed that the force-test thrust coefficients C_T at the operating V/nD of 1.2 for the 26° blade-angle setting varied from $C_T = 0.0125$ to $C_T = 0.0170$ depending on the position of the survey rake. The force-test thrust coefficient for the condition of V/nD of 2.8 and the blade-angle setting of 53° varied from 0.0725 to 0.0800. This change in thrust coefficient with rake position suggests that there is a blocking effect which changes with rake position. This blocking effectively changes the velocity in the plane of the propeller and thus the operating V/nD of the propeller. Therefore comparisons made at the same V/nD with theoretical calculations based on free-air conditions would not be expected to be in exact agreement. With this consideration in mind the agreement between experiment and theory is good.

The shift in the position of the maximum force between the experimental and calculated data noted particularly in figure 5 is due to several factors. First, the survey rake for the experimental data was 18 inches (0.375 propeller diameter) behind the center line of the propeller. Calculations showed that, in this distance, the twist of the propeller slipstream accounted for approximately 12° shift of the maximum

force for the operating condition of $\frac{V}{nD} = 1.2$ and $\beta = 26^\circ$ but was

negligible for the operating condition of $\frac{V}{nD} = 3.1$ and $\beta = 53^\circ$.

Second, the unsteady flow on the blade sections causes a lag in the forces (about 5°) which means that the maximum force does not occur on the horizontal as would be indicated from steady-flow calculations. This lag in the position of the maximum force is a function of the frequency of the oscillation and decreases with the propeller rotational speed, which means that it would decrease as the V/nD is increased for constant forward speed. Third, the inclusion of the flapping of the blade section in the calculations causes an additional lag in the position of the maximum force (about 16°).

Figure 8 shows calculated differential thrust-coefficient curves of a two-blade propeller for three blade positions for the 26° blade-angle

setting operating at a V/nD of 1.2 and with the thrust axis inclined 4° to the air stream. The experimental curves for two positions for a 30° lag in phase angle are shown for comparison. The calculated distribution of thrust coefficient with radius is in good agreement with the experimental distribution.

Forces computed by oscillating-airfoil theory. - Figures 9 to 12 show the results of some of the calculations made for an oscillating airfoil in a pulsating flow field in incompressible flow. The results for all the curves in these figures apply to any particular blade section. The total force on the propeller blade for any blade position is found by summing up the forces along the blade.

The variation of L_c with ωt is shown in figure 9 at $\epsilon = 0.10$ for several values of k with the steady part of the angle of attack α equal to zero. In any particular case, the quantity k is fixed by the operating conditions of the propeller and by the blade chord. Interpreted physically, the quantity $1/k$ is a measure of the wave length between successive waves in the vortex wake in terms of the half-chord; in the steady-state calculations this wave length is arbitrarily assumed to be very large with respect to the chord. Thus, in figure 9 the curve of L_c against ωt at $k = 0$ shows the results obtained for assumed steady-state conditions in potential flow. The curves in figure 9 for other values of k show that the effect of the oscillations is to modify the forces as obtained from the assumption of steady-state conditions. Presumably, a similar effect would occur in a compressible flow.

The asymmetry of the curves for L_c in figure 9 is caused primarily by the variation in the dynamic pressure $\frac{1}{2}\rho W_{\omega t}^2$ during the cycle. This asymmetry may be also seen in figure 10, which shows the variation at $k = 0.10$ of L_c with ωt with ϵ as parameter for several values of α/α_{P_0} . The curves for $\epsilon = 0$ are the most nearly symmetrical; this condition corresponds to Theodorsen's case of an airfoil oscillating in a steady flow (reference 1). It can be seen from figure 10 that the amplitude of the lift variation tends to increase as ϵ increases and also that this amplitude increase is further accentuated by increasing the initial load at $\omega t = 0$ (α/α_{P_0} increasing). Figure 11 shows the variation of the force coefficients for $\omega t = 90^\circ$ and for $\omega t = 270^\circ$ for several values of ϵ for $\frac{\alpha}{\alpha_{P_0}} = 0$. In the same figure are values of $(L_{c90} - L_{c270})$ which are a measure of the maximum bending moment on

the shaft axis of a two-blade propeller (divided by 2 for convenience of plotting). The absolute magnitude of the maximum force coefficients varies greatly as the value of ϵ is increased, but the variation of the difference in the forces from the heavily loaded side to the lightly loaded side which gives the bending moment is small.

Figure 12 shows the variation of L_c at 90° and 270° with k at several values of α/α_{P_0} with $\epsilon = 0$. In this special case it is seen that the magnitude of the loading increases as α/α_{P_0} is increased but

that the bending load factor $\frac{L_{c90} - L_{c270}}{2}$ is independent of initial loading on the blade section. This independence does not hold in a pulsating flow field as may be seen in figure 13, which shows the vari-

ation of the bending load factor $\frac{L_{c90} - L_{c270}}{2}$ with k at several values of $\epsilon \frac{\alpha}{\alpha_{P_0}}$.

Figure 14 shows the variation in the turning-moment coefficient on the inclined propeller shaft (yawing moment for pitched propeller) of the NACA 4-(3.9)(07)-0345-B propeller. These coefficients were calculated by the oscillating-flow theory and are considerably lower than the moments calculated by assuming steady-state conditions at each phase angle and using compressible airfoil characteristics. The curves are only useful in showing the variation of the moments with the time variable ωt and not the absolute magnitude. The variation of the turning-moment coefficient with time for a two-blade propeller operating at a V/ND of 1.2, $\alpha_T = 4^\circ$, and $\beta = 26^\circ$ is shown by the solid curve and for a three-blade propeller by the dashed curve. It is seen that the moment coefficient for a two-blade propeller varies from approximately zero when the blades are in the vertical position to a maximum of 0.0021 when the blades are approximately on the horizontal (twice per revolution). For the same operating condition for the three-blade propeller the moment coefficient remains very nearly constant at approximately 0.0016 (varying between 0.0015 and 0.0017).

Combined steady and oscillating forces. - From the standpoint of theory a combination of the steady-state and the oscillating-airfoil theories approaches the actual operating conditions of the pitched or yawed propeller. The forces or moments are computed by the steady-state methods including compressibility and downwash. The oscillating-airfoil theory is then used to modify these forces. For a two-blade propeller,

the maximum force difference $(L_{90} - L_{270})$ at each section as computed from steady-state calculations with compressible airfoil characteristics would be reduced by a factor which is the ratio of $(L_{c90} - L_{c270})$ at the operating values of k to its value at $k = 0$ (from fig. 13). From figure 13 it will be noticed that, properly, the operating value of $\epsilon \frac{\alpha}{\alpha_{P_0}}$ should also be taken into account; within the limits given in the

figure, however, the ratio $\frac{(L_{c90} - L_{c270})_k}{(L_{c90} - L_{c270})_{k=0}}$ changes only slightly with $\epsilon \frac{\alpha}{\alpha_{P_0}}$.

Figure 15 shows the calculated distribution of the moment coefficient along the radius for the two-blade NACA 4-(3.9)(07)-0345-B propeller with the blades in the horizontal position, with the thrust axis inclined at 4° , with the propeller blade angle set at 26° at the 0.75 radius, and operating at a V/nD of 1.2. The moment coefficients are computed for steady-state conditions in compressible flow and for an oscillating airfoil by the oscillating-airfoil theory. An integration of these curves gives the total turning moment on the propeller shaft. The correction for each radius as obtained from figure 13 has been applied to the steady-state calculations. This correction does not bring the curves into agreement because of the differences in the airfoil characteristics used.

CONCLUSIONS

Methods have been developed to determine the air forces acting on yawed or pitched propellers. At the present time the lack of extensive experimental data precludes conclusive verification of the theoretical considerations presented in this paper, particularly in regard to the applicability of the combined steady-state compressible and oscillating incompressible theory. The comparisons and calculations made, however, indicated the following conclusions:

1. The steady-state method for calculating the propeller forces gives satisfactorily accurate results.
2. The results from the oscillating-flow theory indicate that the actual forces on the blade are somewhat lower than the values calculated by the steady-state method, particularly at low advance ratios.

3. The turning moment on the shaft of a two-blade propeller fluctuates between approximately zero and its maximum value twice per revolution.

4. For the operating condition investigated the turning moment on the shaft of the three-blade propeller remains nearly constant at about 75 percent of the maximum value attained with the two-blade propeller.

Langley Aeronautical Laboratory
National Advisory Committee for Aeronautics
Langley Field, Va., December 20, 1948

REFERENCES

1. Theodorsen, Theodore: General Theory of Aerodynamic Instability and the Mechanism of Flutter. NACA Rep. 496, 1935.
2. Greenberg, J. Mayo: Airfoil in Sinusoidal Motion in a Pulsating Stream. NACA TN 1326, 1947.
3. Pendley, Robert E.: Effect of Propeller-Axis Angle of Attack on Thrust Distribution over the Propeller Disk in Relation to Wake-Survey Measurement of Thrust. NACA ARR I5J02b, 1945.
4. Crigler, John L.: Comparison of Calculated and Experimental Propeller Characteristics for Four-, Six-, and Eight-Blade Single-Rotating Propellers. NACA ACR 4B04, 1944.
5. Stack, John: Tests of Airfoils Designed to Delay the Compressibility Burble. NACA Rep. 763, 1943.

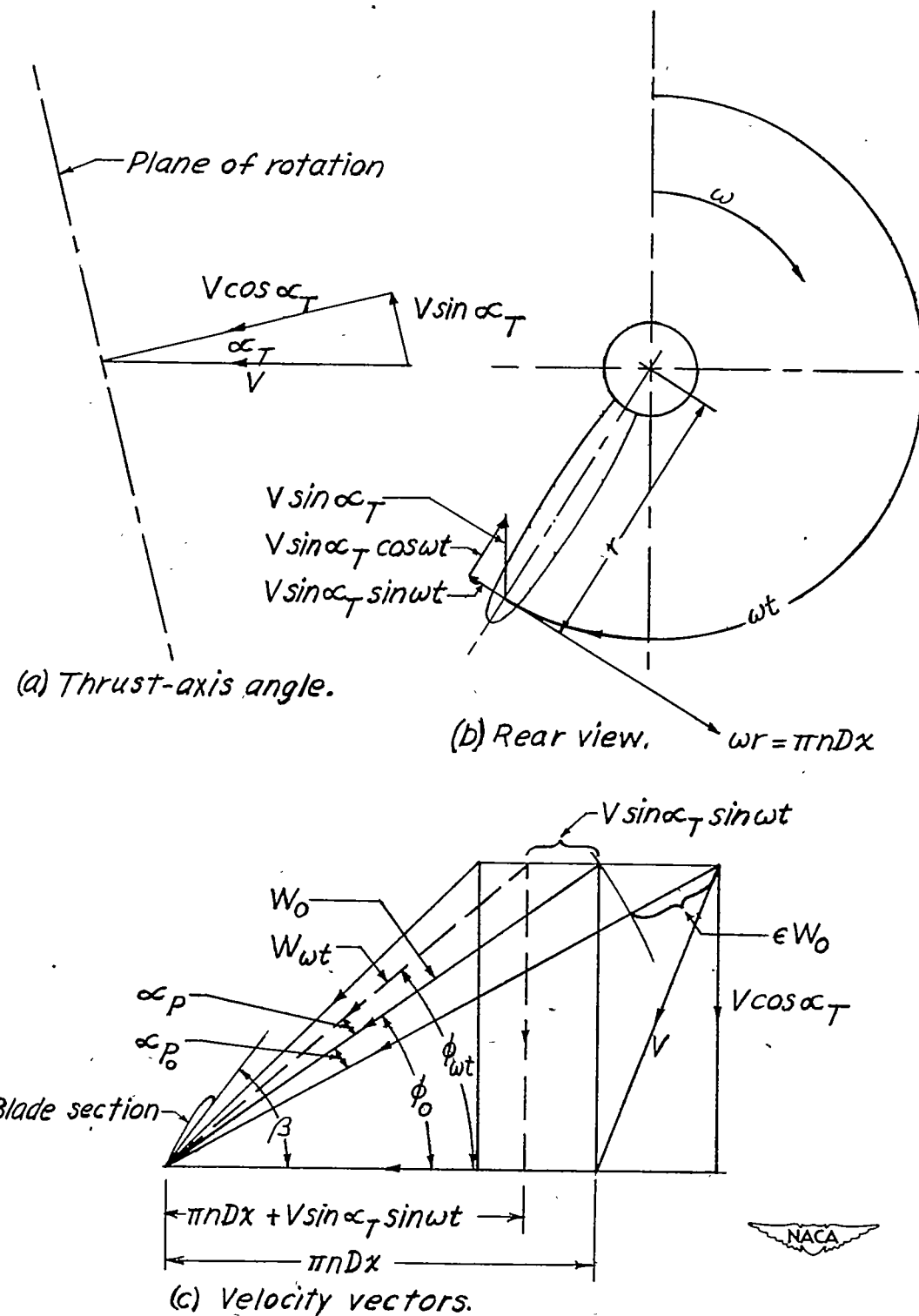


Figure 1.— Velocity diagram of inclined propeller.

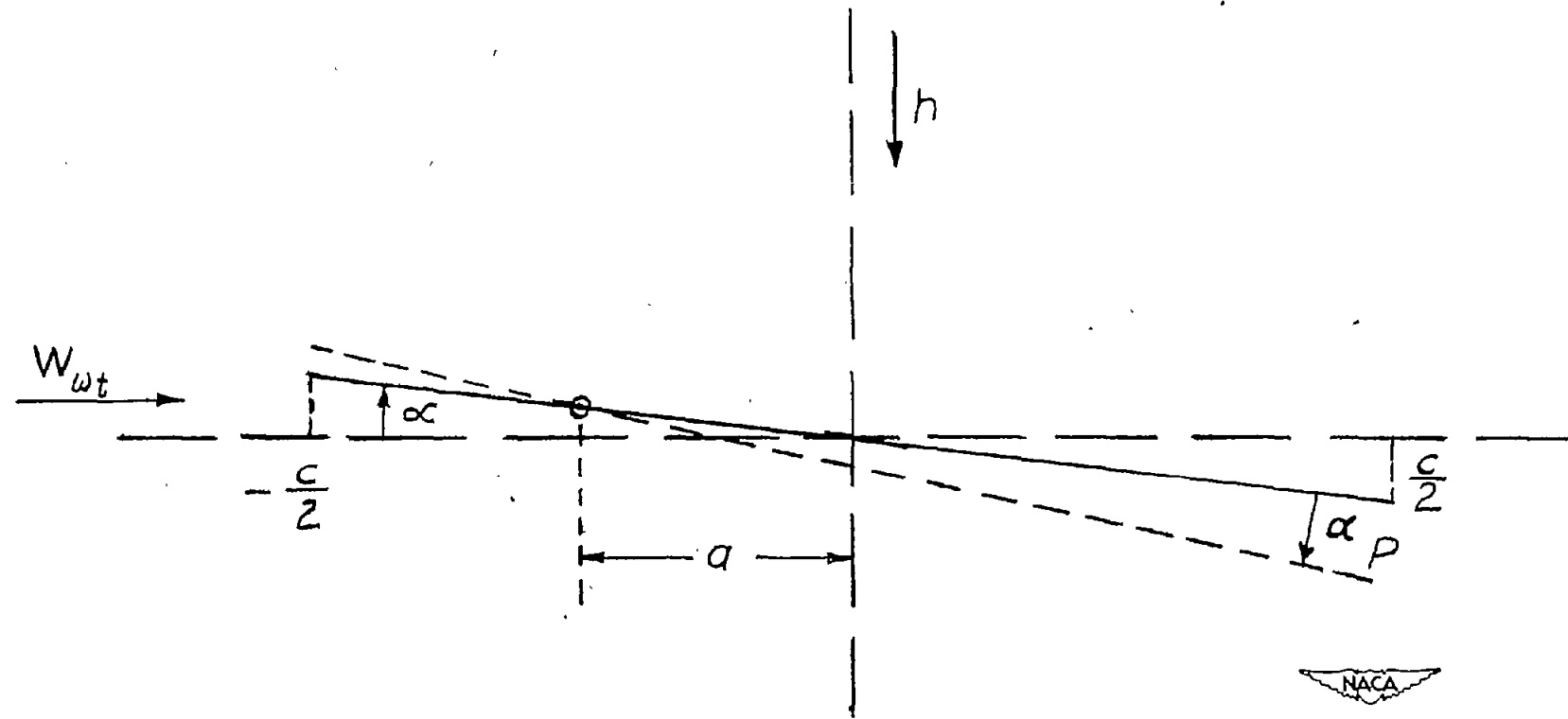


Figure 2.— Diagram showing notation used for oscillating airfoil in unsteady flow (from reference 2).

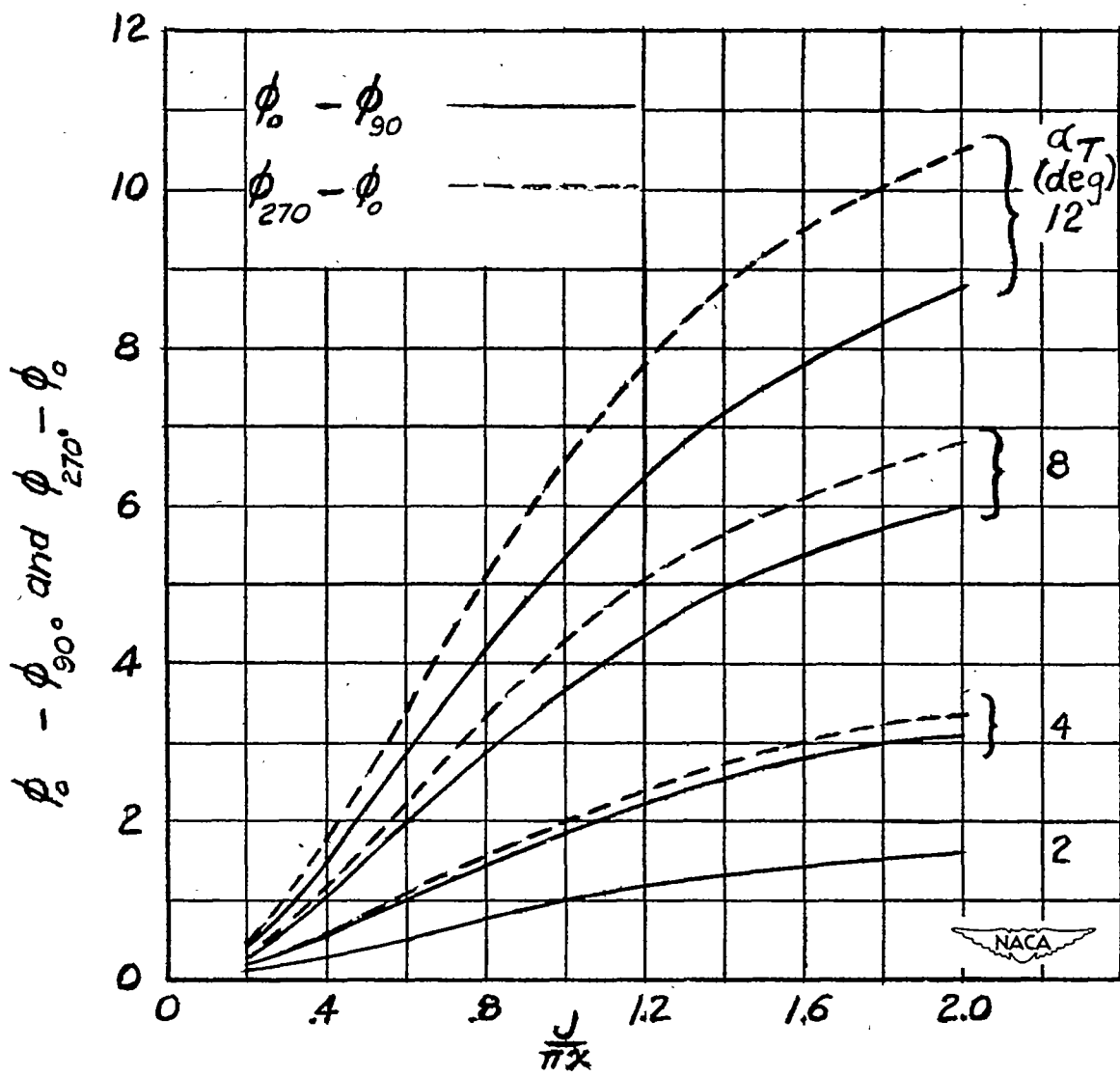


Figure 3.— Variation in amplitude of geometric angle of attack.

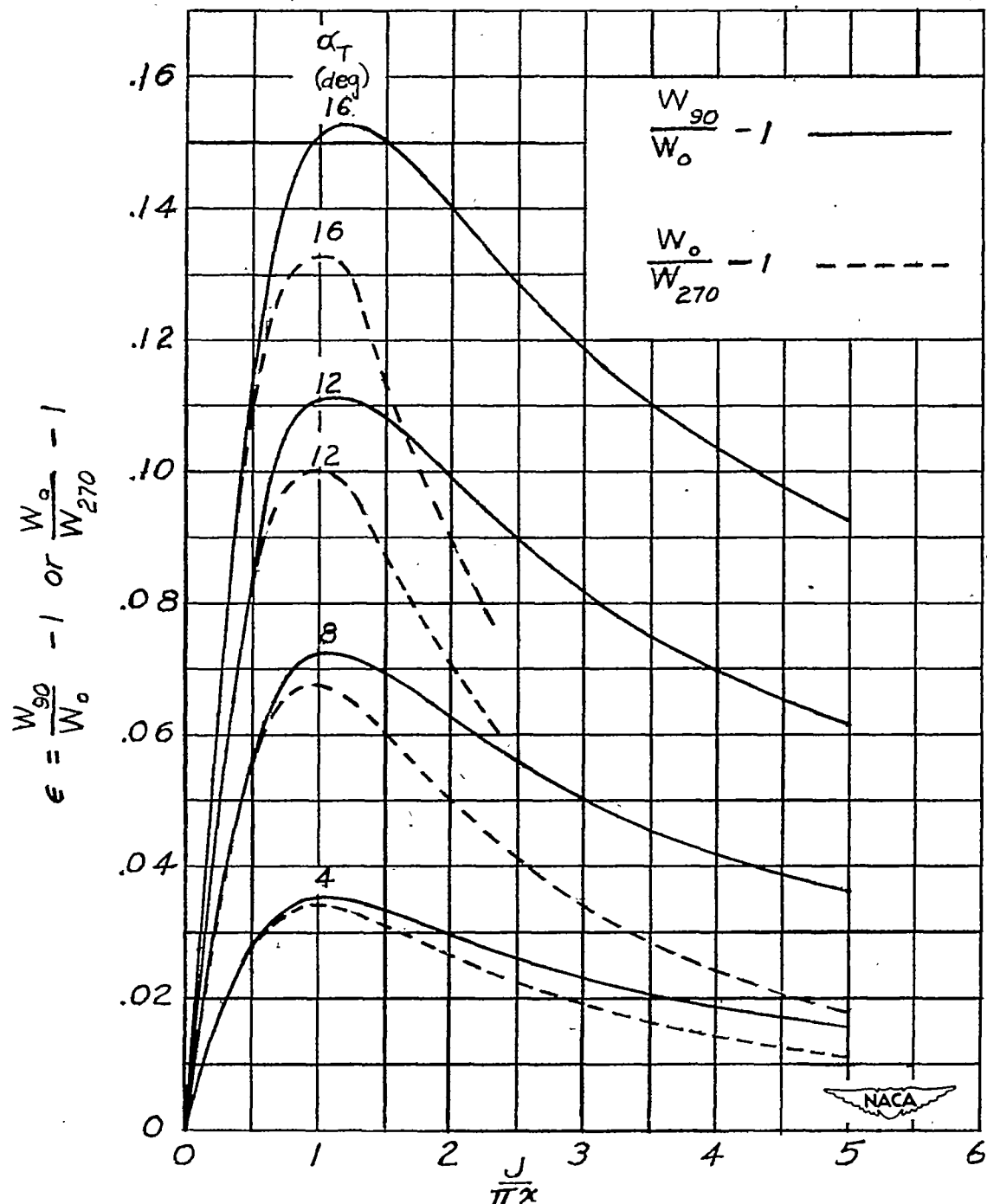


Figure 4.— Variation in fractional amplitude of resultant velocity.

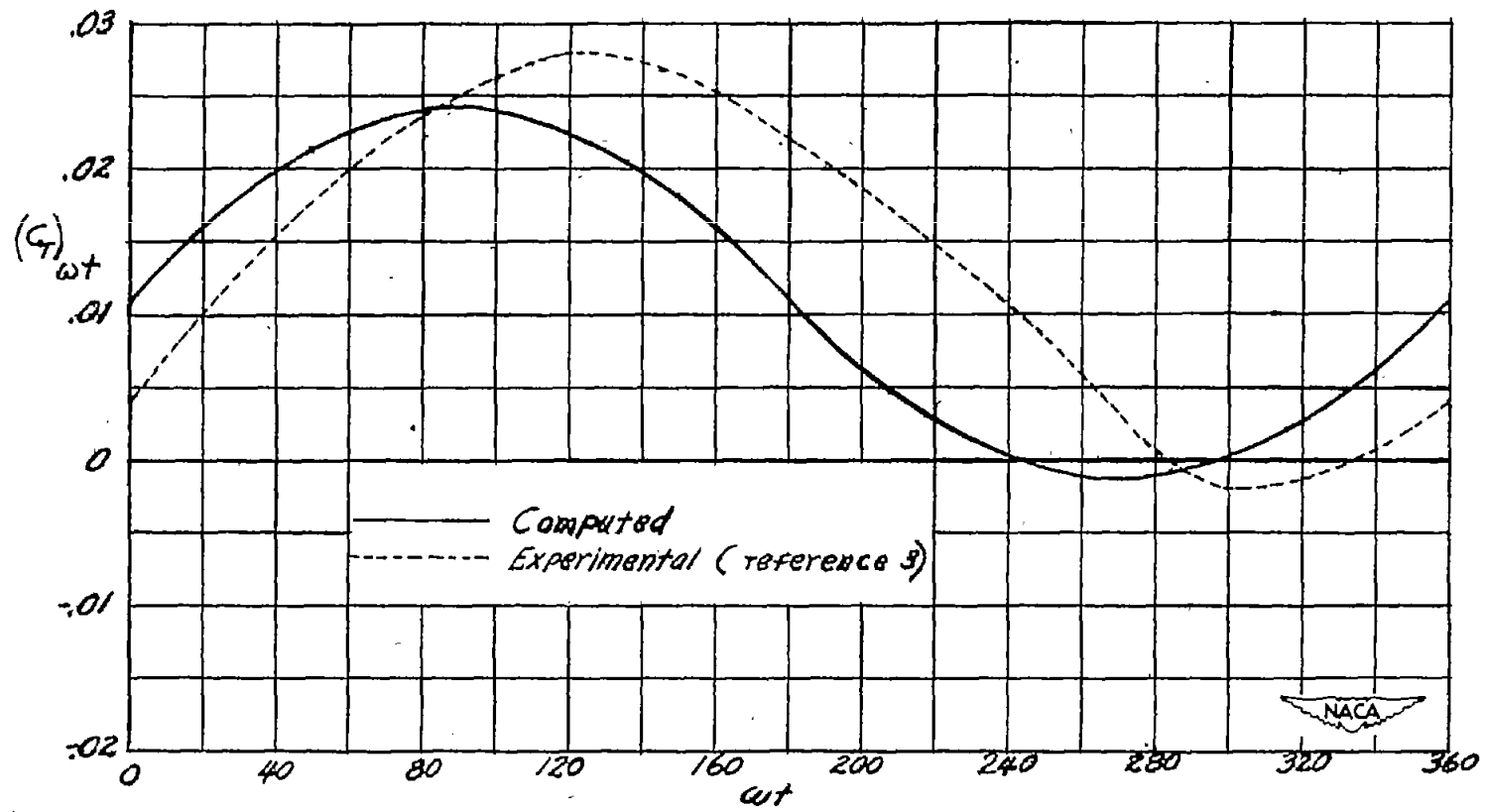


Figure 5.— Variation of instantaneous thrust coefficient with blade position. $B, 2; \beta, 26^\circ; J, 1.2;$
 $\alpha_T, 4^\circ$.

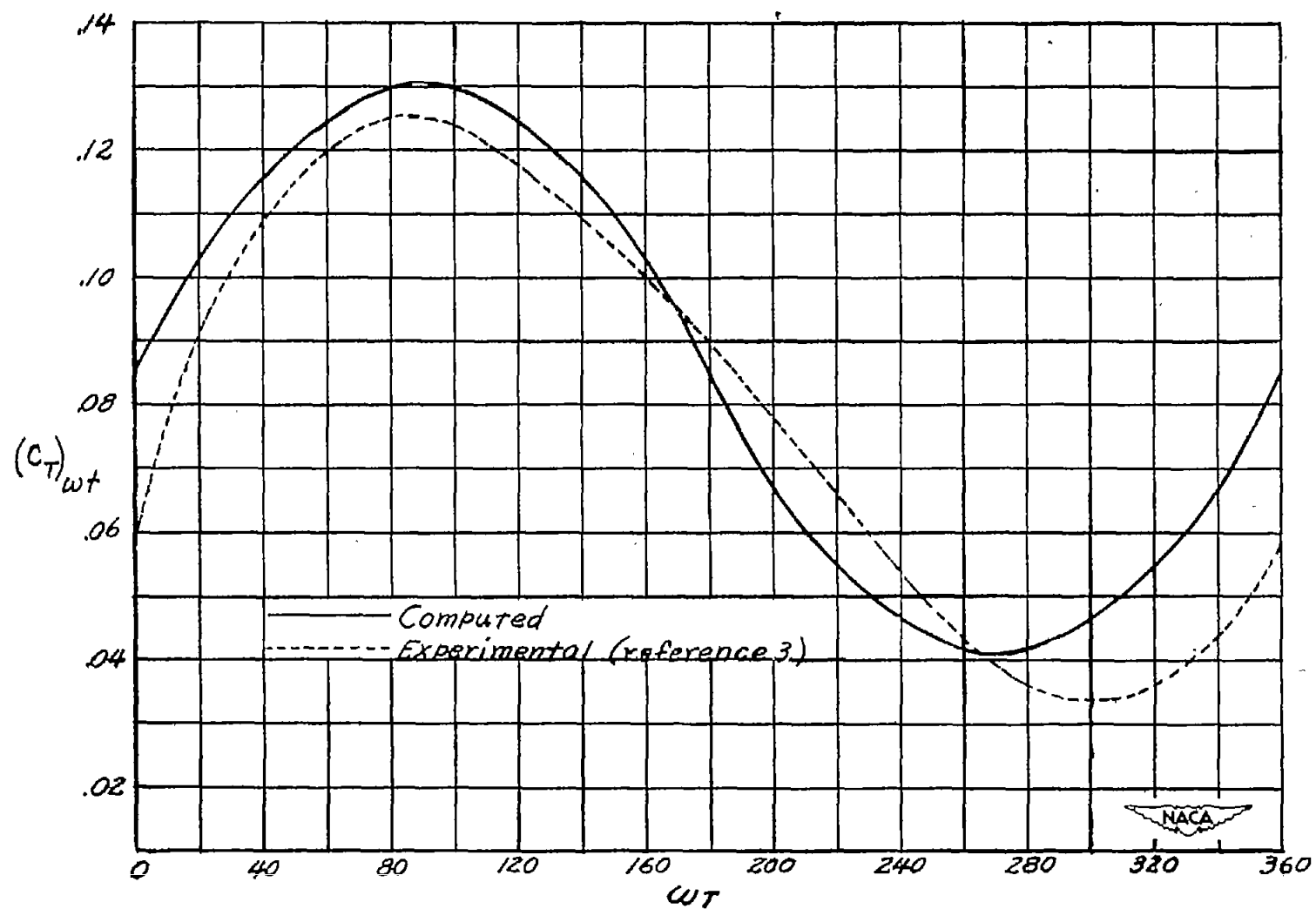


Figure 6.— Variation of instantaneous thrust coefficient with blade position. $B, 2; \beta, 53^\circ; J, 2.8;$
 $\alpha_T, 40^\circ.$

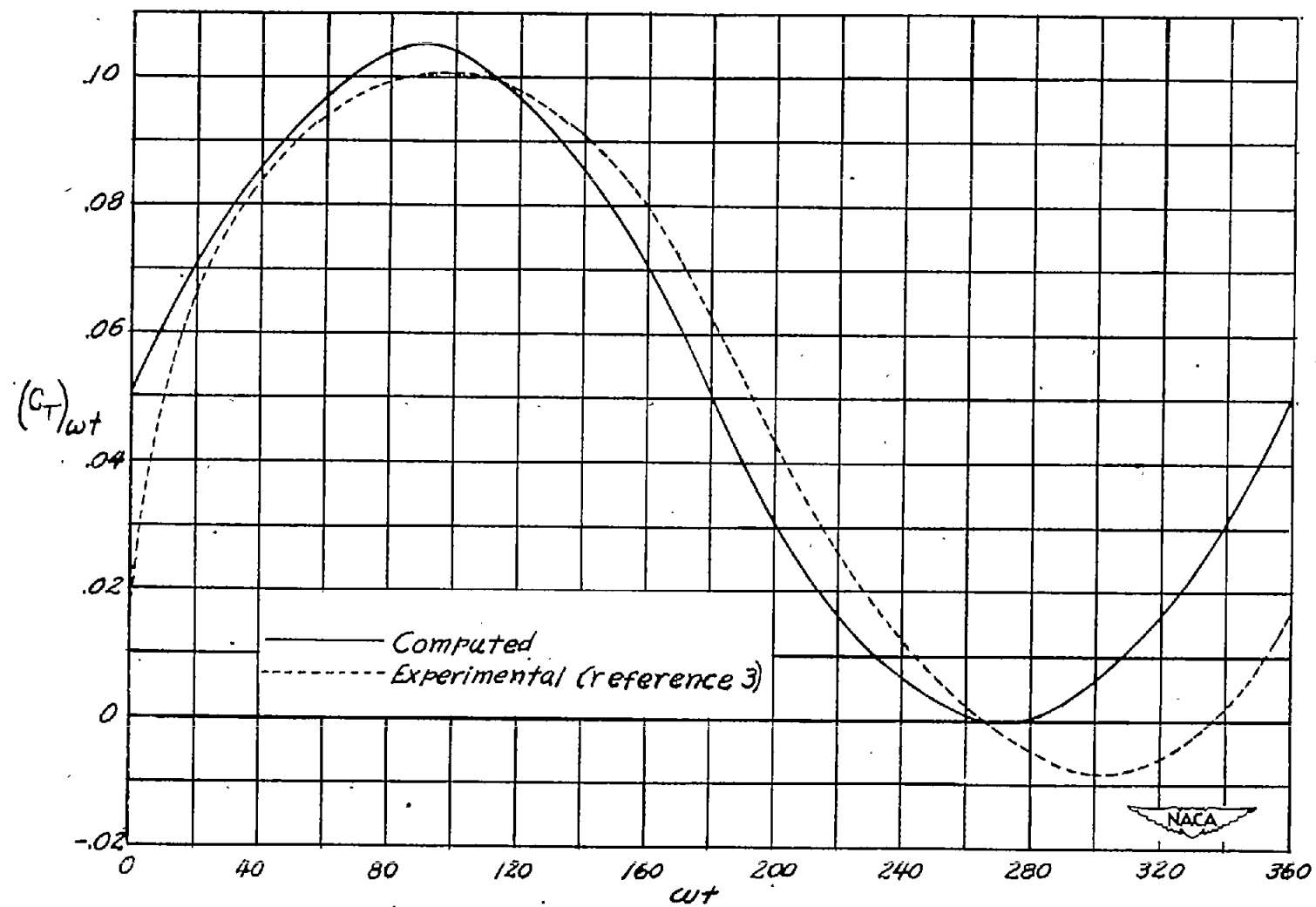


Figure 7.— Variation of instantaneous thrust coefficient with blade position. B,2; $\beta, 53^\circ$; J,3.1; $\alpha_T, 40^\circ$.

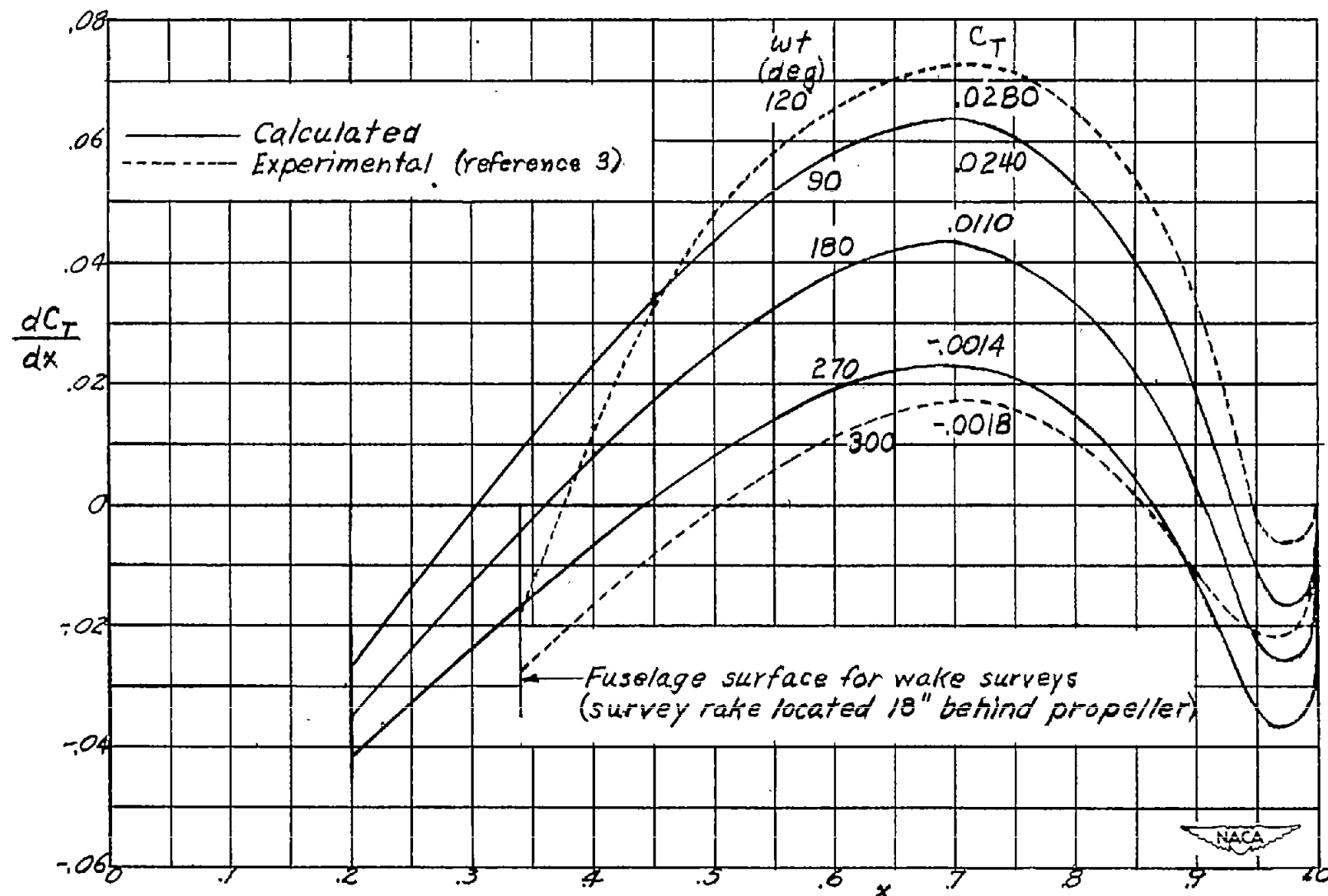


Figure 8.— Thrust gradient curves for three blade positions. $B, 2; \beta, 26^\circ; J, 1.2; \alpha_T, 4^\circ$.

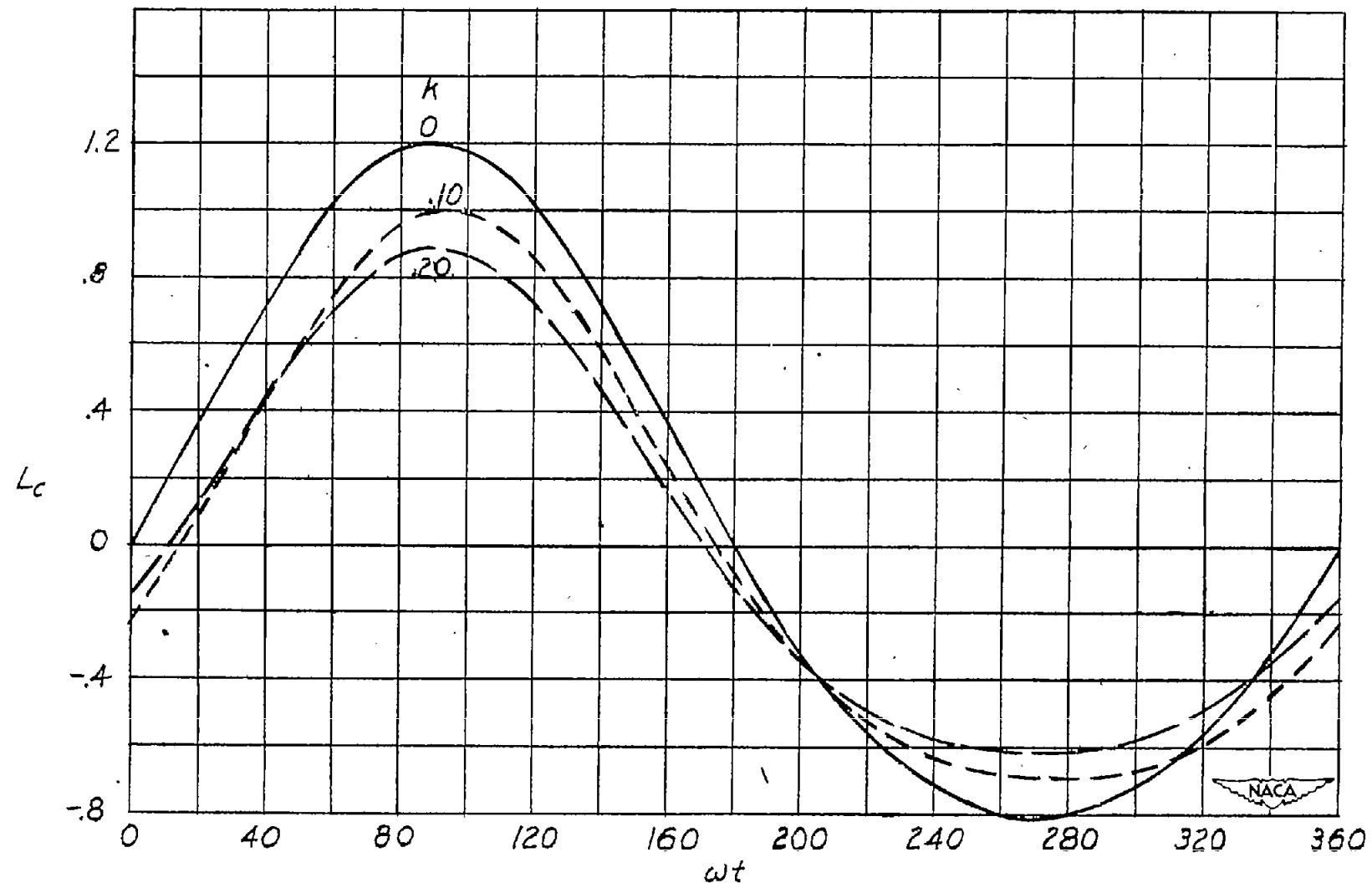


Figure 9.- Variation of force coefficient with blade position. $\epsilon, 0.10; \frac{a}{a_{P_0}}, 0.$

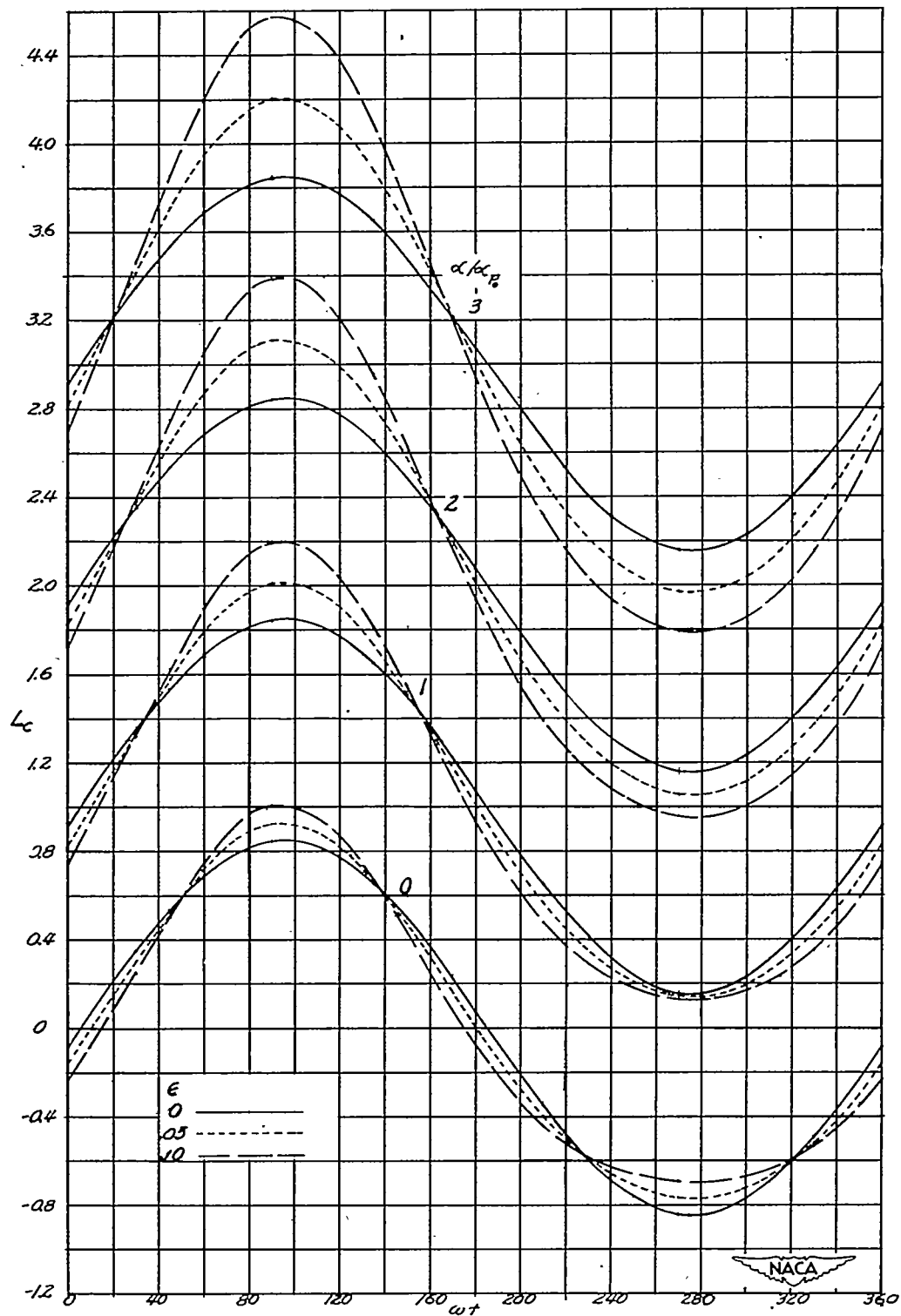


Figure 10.- Variation of force coefficient with blade position. $k, 0.10.$

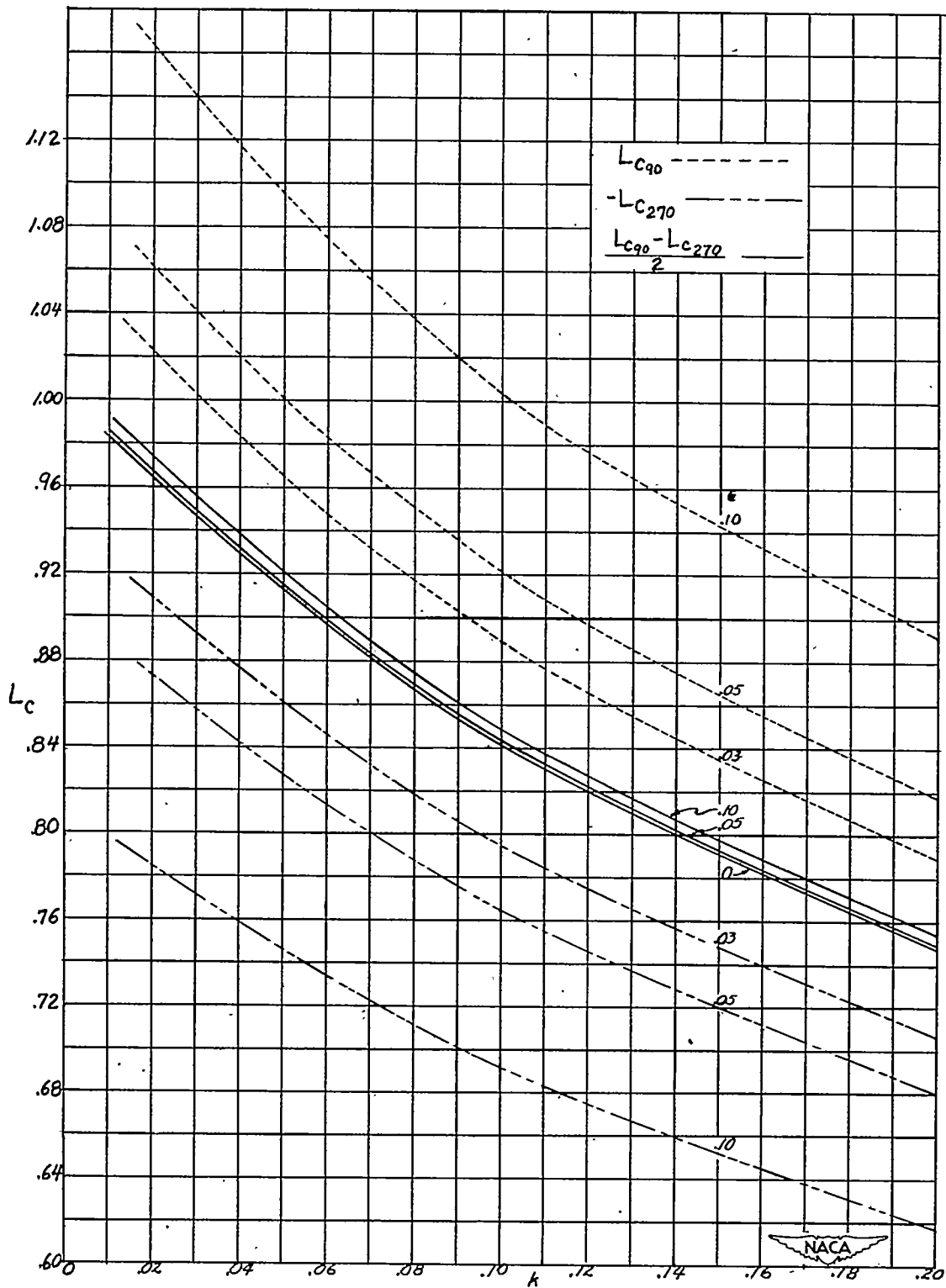


Figure 11.-- Variation of force coefficient with k . $\frac{\alpha}{\alpha_{P_0}} = 0.$

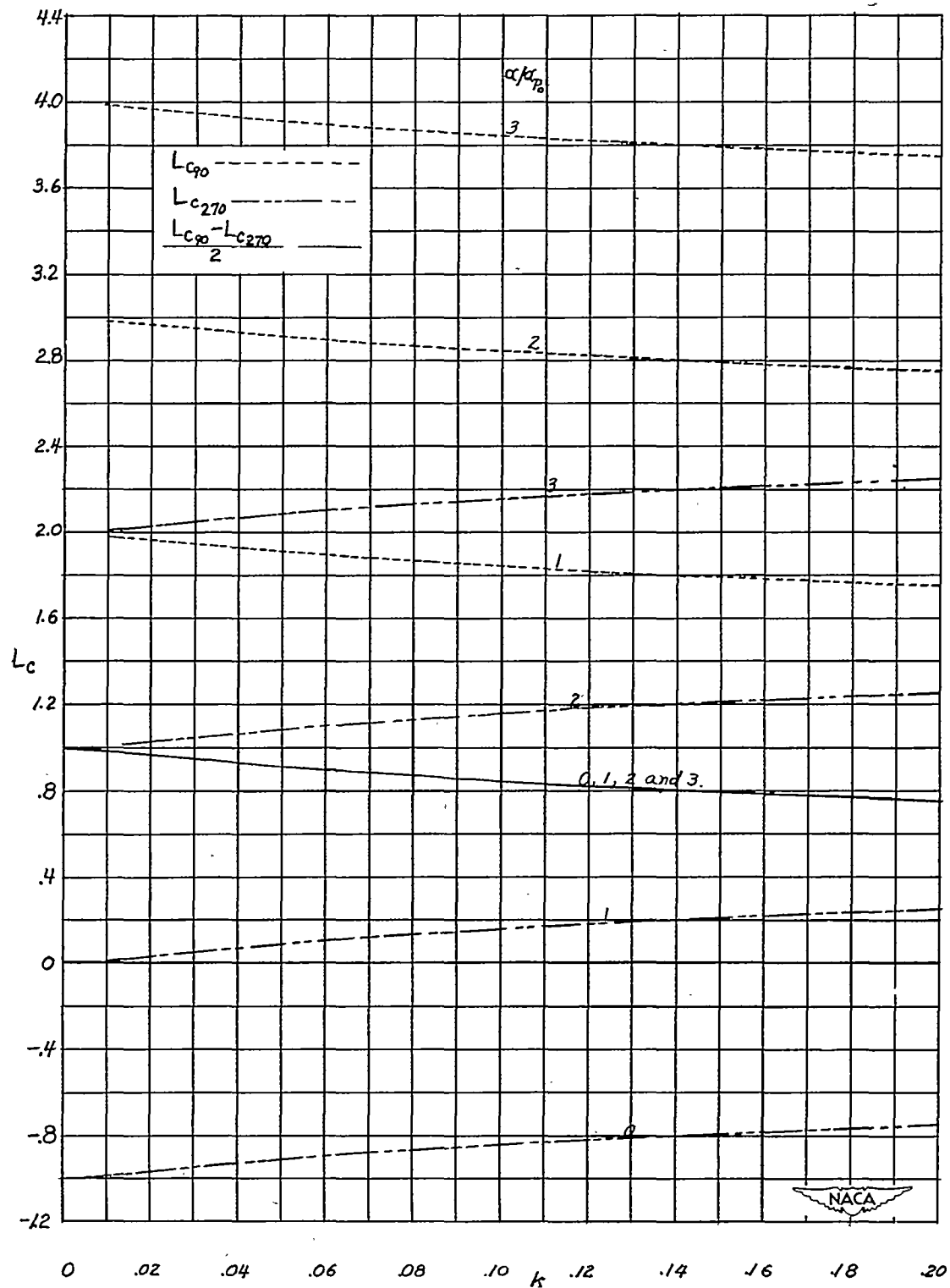


Figure 12.— Variation of force coefficient with k . $\epsilon = 0$.

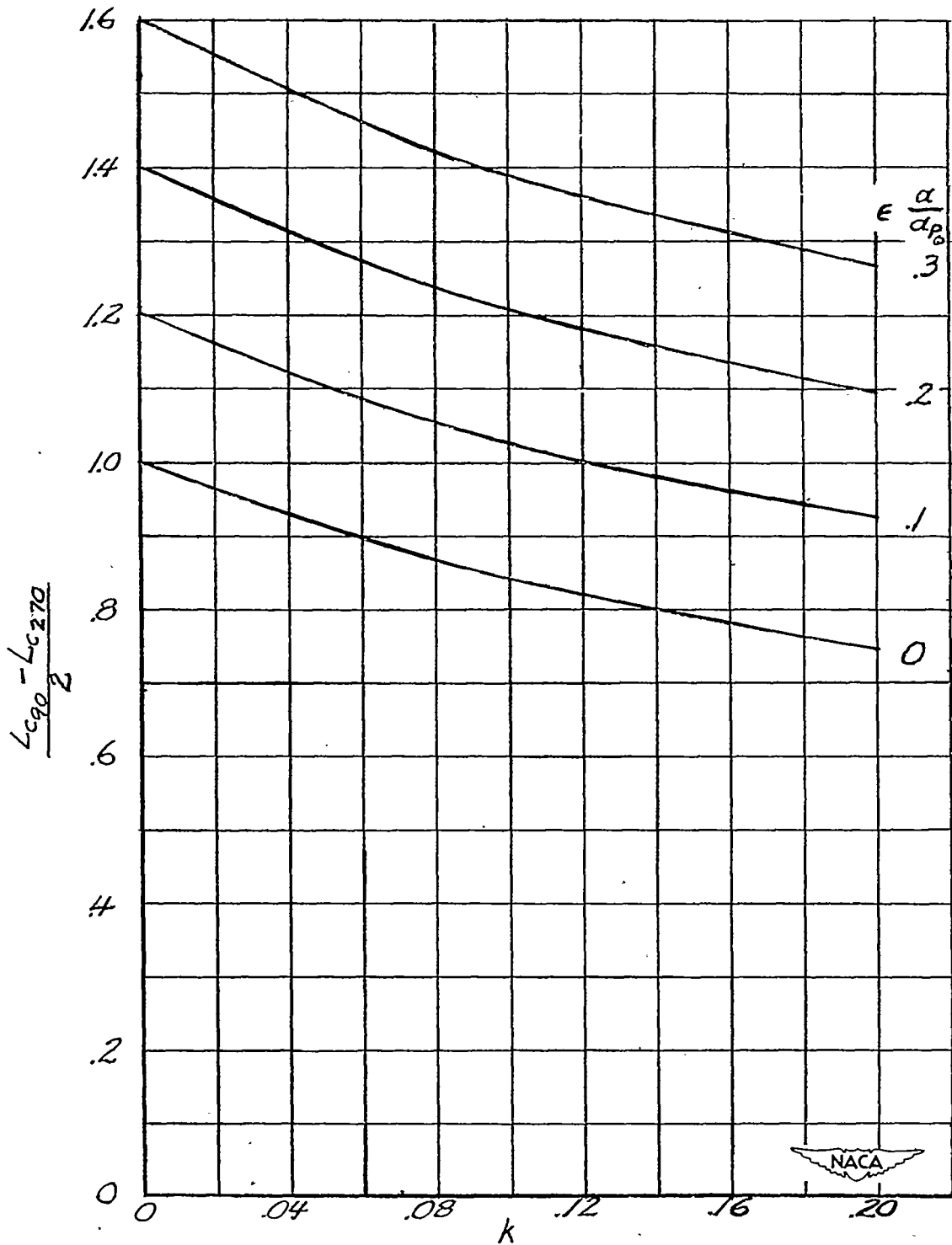


Figure 13.— Variation of force coefficient with k and with $\epsilon \frac{\alpha}{\alpha_{p_0}}$.
 $(\epsilon < 0.1)$.

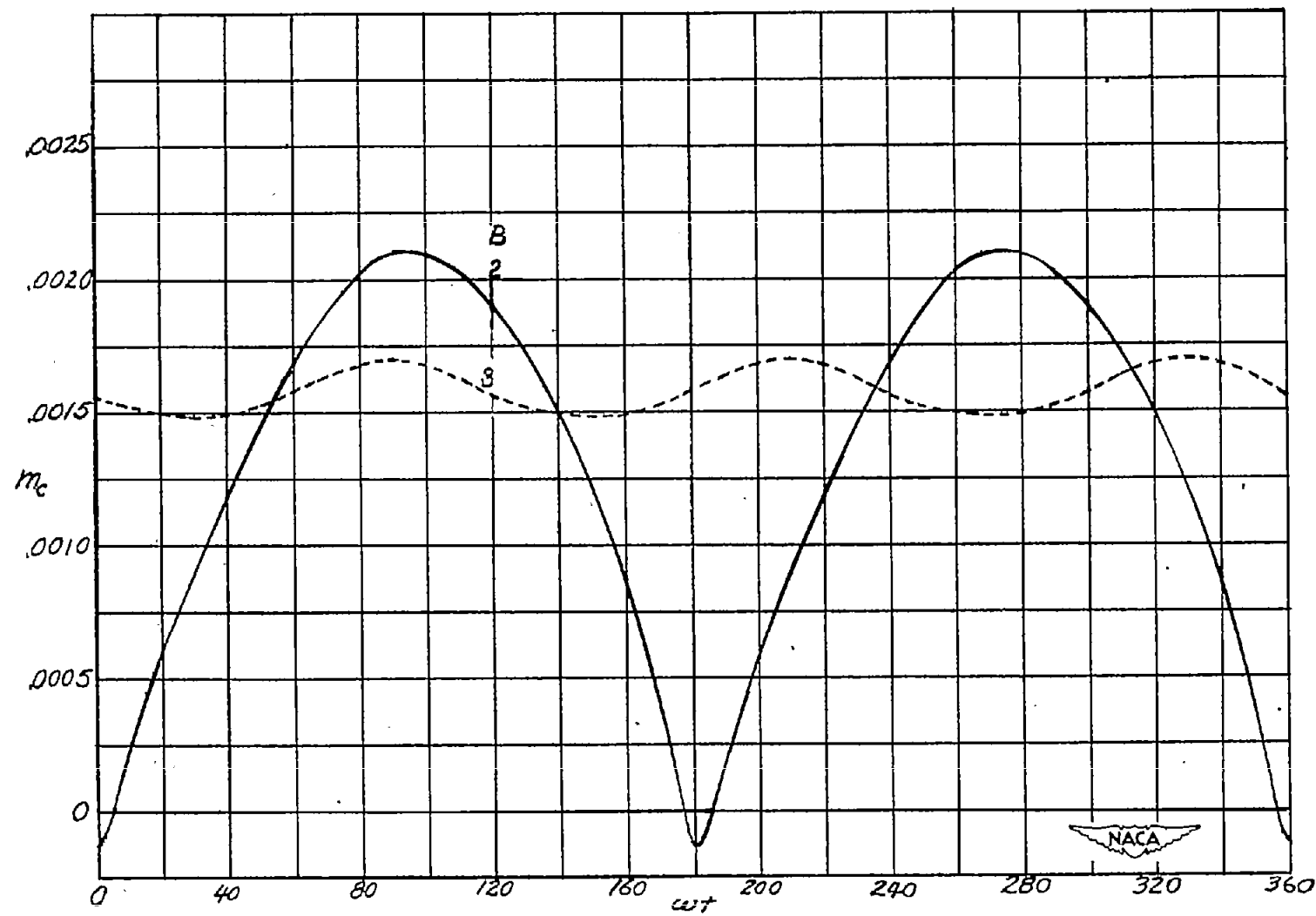


Figure 14.— Variation of bending-moment coefficient with blade position. Propeller 4-(3.9)(07)-0345-B.
 $\beta, 26^\circ$; J, 1.2; $a_T, 4^\circ$.

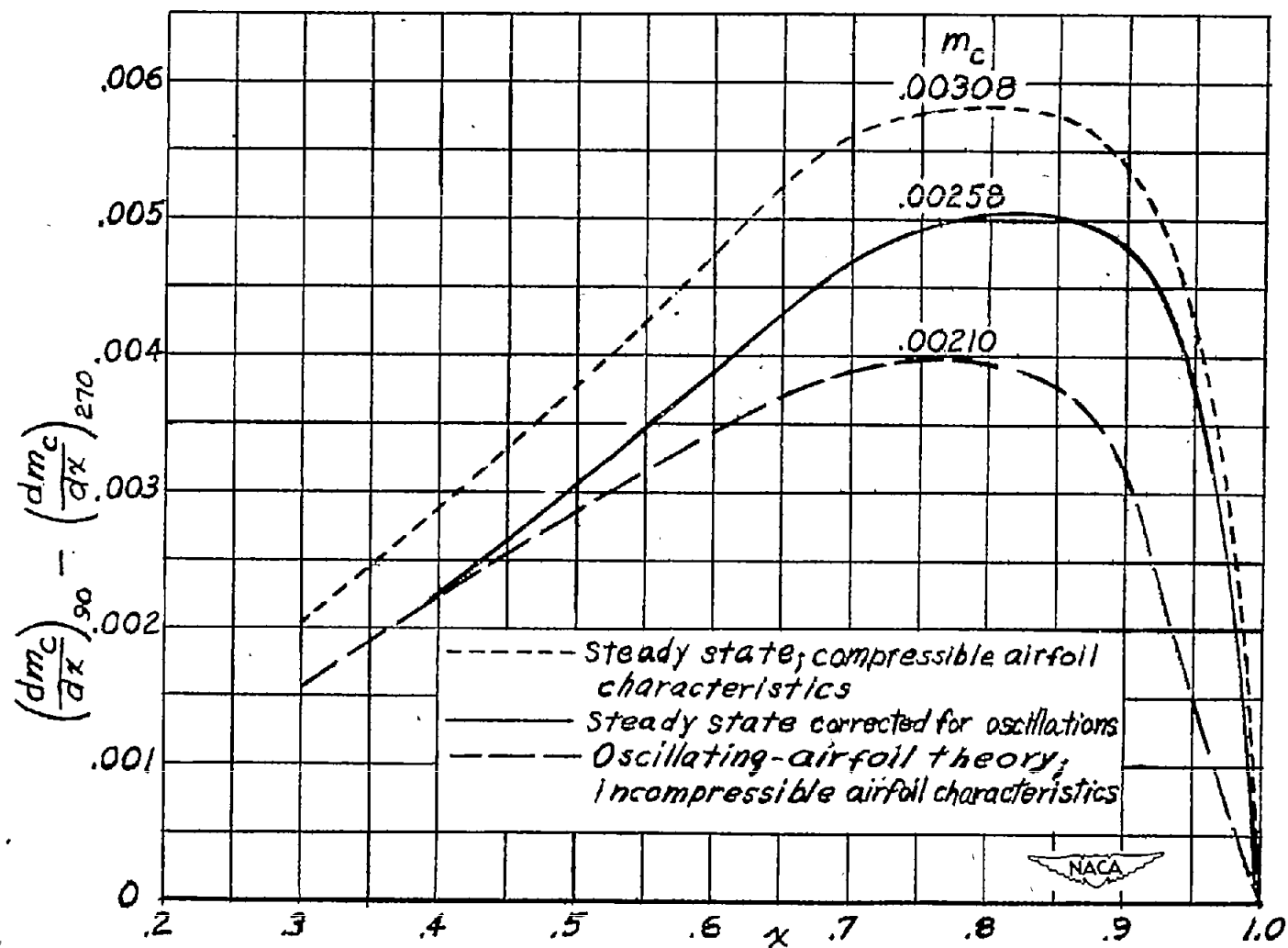


Figure 15.— Distribution of maximum bending-moment coefficient for propeller 4-(3.9)(07)-0345-B.
 $\beta, 26^\circ$; $J, 1.2$; $a_T, 4^\circ$; $B, 2$.